PHYSICAL REVIEW A **91**, 053405 (2015)

Core-shell magneto-optical trap for alkaline-earth-metal-like atoms

Jeongwon Lee, Jae Hoon Lee, Jiho Noh, and Jongchul Mun
Korea Research Institute of Standards and Science, Daejeon 305-340, Korea

(Received 5 January 2015; published 8 May 2015)

We propose and demonstrate a type of magneto-optical trap (MOT) for alkaline-earth-metal-like (AEML) atoms where the narrow intercombination ${}^1S_0 \rightarrow {}^3P_1$ transition and the broad ${}^1S_0 \rightarrow {}^1P_1$ transition are spatially arranged into a core-shell configuration. Our scheme resolves the main limitations of previously adopted MOT schemes for AEML atoms, leading to significant increases in both the loading rate and the steady-state atom number. We apply this scheme to our experimental setup with ^{174}Yb atoms and observe more than two orders of magnitude improvement in the loading rate and tenfold improvement in the steady-state atom number compared to a conventional intercombination MOT scheme. This technique could be readily extended to other AEML atoms to increase the statistical sensitivity of many different types of precision experiments.

DOI: 10.1103/PhysRevA.91.053405 PACS number(s): 37.10.De, 37.10.Gh

I. INTRODUCTION

Alkaline-earth-metal-like (AEML) atoms with two valence electrons have received great interest in various fields [1–12] due to their spinless ground state ${}^1S_0$ and a long-lived metastable state ${}^3P_0$. More specifically, precision spectroscopy of lattice-trapped AEML atoms opened up many possibilities such as optical clocks [1–3], gravimeters [4], and, most recently, the exploration of SU(N) magnetism [5,6]. Another branch of experiment uses laser-cooled AEML atoms to search for the permanent electric dipole moment [11,12]. For many of these precision-measurement experiments, increasing the atom number in the cold atomic sample and/or reducing the preparation time directly affect the statistical sensitivity. Therefore, a fast-loading magneto-optical trap (MOT) with high atom numbers becomes desirable.

AEML atoms have two commonly used laser-cooling transitions, which are the broad ${}^1S_0 \rightarrow {}^1P_1$ transition (which we refer to as the singlet transition) and the narrow ${}^1S_0 \rightarrow {}^3P_1$ transition (which we refer to as the triplet transition). Figure 1(a) shows the singlet and triplet transitions for Yb, a well-known representative of AEML atoms. Due to the broader natural linewidth of the singlet transition in AEML atoms, higher capture velocity and faster loading is allowed for a MOT using the singlet transition (singlet MOT) compared to the triplet transition (triplet MOT). On the other hand, the triplet MOT has advantages over the singlet MOT in terms of lower Doppler temperature limit and closed cycling of the cooling transition [13].

There have been two main approaches for efficient loading of AEML atoms into a MOT. One way is to initially load a singlet MOT with a certain magnetic field gradient, and subsequently transfer to a triplet MOT with a different magnetic field gradient [14]. While one could achieve faster loading using this transfer technique, the steady-state atom number of the singlet MOT is limited by the branching ratio of the ${}^1P_1$ state decaying to the metastable triplet states. Therefore, to date, the maximum number of trapped atoms for ^{174}Yb has been limited to the 10^7 range, even with high transfer efficiencies [15]. A singlet MOT repumping scheme was proposed for Yb to remedy the loss of atoms into the metastable triplet states. However, only a limited gain in the atom number of 30% was reported [16]. More recently, a buffer gas source loaded Yb singlet MOT was demonstrated with higher loading rates [17]; however, the case of MOT lifetime was limited to few tens of milliseconds and transfer to a triplet MOT has not been achieved. A second approach is to artificially frequency broaden the triplet cooling laser light via modulation in order to increase the capture velocity [13]. Although this broadband technique results in slower loading compared to the transfer technique, the absence of leaky channels in the triplet-transition cooling process allows for higher numbers of trapped atoms above the 10^8 range [18].

In this paper, we introduce a core-shell MOT scheme for AEML atoms and experimentally demonstrate its capabilities with ^{174}Yb atoms. Results show that this scheme produces a faster-loading MOT with higher steady-state atom numbers compared to previous schemes. We use the broadband triplet cooling light at the central core part of the MOT (BB triplet core), and surround it with a shell of the singlet cooling light (singlet shell). Unlike the singlet-triplet MOT transfer scheme, we fix the magnetic field gradient at an optimum value throughout the cooling process. This arrangement of the light fields allows us to take advantage of the different properties of the two cooling transitions. The singlet shell with a relatively higher capture velocity increases the MOT loading rate, complementing the BB triplet core with lower capture velocity. The atoms in the singlet shell are then pushed into the BB triplet core, where they are further cooled without any limitations caused from the branching ratio mentioned above.

II. EXPERIMENTAL METHODS

Our experimental setup is shown in Fig. 1(b), which consists of an atomic-beam source, spin-flip Zeeman slower, and the core-shell MOT. We begin the experiment by heating Yb chunks up to 400 °C inside the oven. The atoms exit the oven as an effusive beam with a mean axial velocity of around 300 m/s after passing through a capillary-type nozzle, which is 10 mm long and 1 mm in diameter. The atomic beam is spatially filtered through a conical-shaped skimmer with a 2-mm-diameter hole. The atomic beam can be turned off in 100 ms with a motorized beam shutter placed between the oven and skimmer. The atoms pass a differential pumping stage before entering a 30-cm-long spin-flip Zeeman slower. The total distance between the oven and the MOT is about

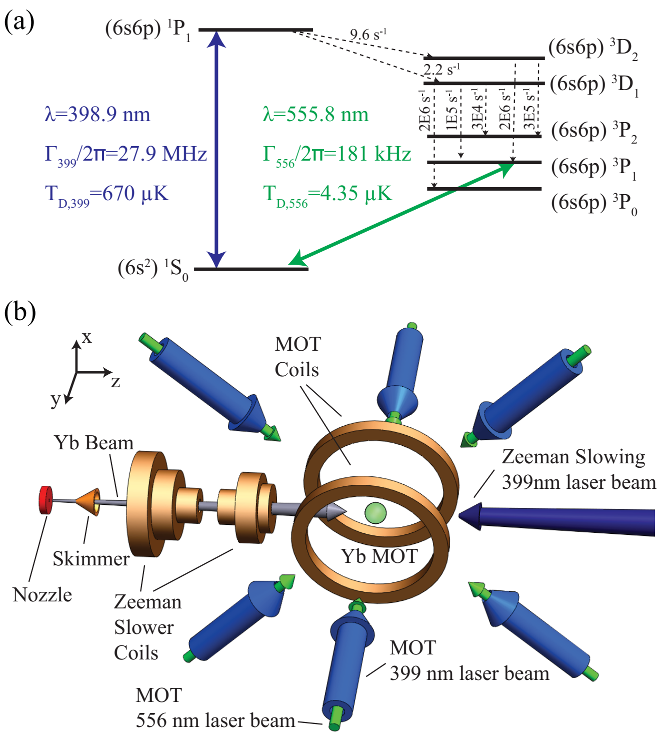

FIG. 1. (Color online) (a) Energy-level diagram of Yb showing the singlet and the triplet laser-cooling transition along with relevant physical properties. Γ is the natural linewidth and T_D is the Doppler temperature of the cooling transition. The dotted line shows the various decay channels of the $^1P_1$ state. (b) Schematic view of the experimental setup for the core-shell magneto-optical trap.

90 cm. Under the beam operation, the vacuum pressures were maintained at $\sim 10^{-8}$ Torr between the nozzle and the skimmer, and $\sim 10^{-11}$ Torr inside the MOT chamber.

The spin-flip Zeeman slower was designed to have a capture velocity of 300 m/s, operated with the singlet transition. An external cavity diode laser was combined with a tapered amplifier to generate 798 nm light, which we frequency doubled with a second harmonic generation unit (Toptica SHG Pro) to get 399 nm light. We use 60 mW of the 399 nm laser beam at a frequency detuning of −640 MHz ($-22\ \Gamma_{399}$) for the Zeeman slower, where Γ_{399} is the on-resonance scattering rate of the singlet transition. The Zeeman slower laser beam counterpropagates with respect to the atomic beam, and is focused down from 10 mm at the MOT center to 1 mm diameter at the oven nozzle in order to match the atomic-beam divergence. The atomic velocity distribution along the z axis after the Zeeman slower was measured to be centered around 25 m/s using laser-induced fluorescence spectroscopy.

After the Zeeman slower, the atoms are captured by the core-shell MOT where we have two spatially separated coaxial laser beams counterpropagating along all three dimensions. For each axis, we use a circular mask with a chosen diameter to block the center of a 10 mm, $1/e^2$ diameter singlet-transition laser beam, while the hole is filled in with a matching $1/e^2$ diameter triplet-transition laser beam using a dichroic mirror. We use a 399 nm diode laser for the singlet shell. The singlet-transition laser-beam powers after the mask were 15 mW for each of the two axes on the x-z plane, and 3 mW along the y axis. As for the BB triplet core, light from a frequency doubled fiber laser (Menlo Orange One and PPLN SHG unit) at 556 nm frequency modulated sinusoidally at 300 kHz (1.66 Γ_{556}) with an acousto-optic modulator, where Γ_{556} is the on-resonance scattering rate for the triplet transition. The power of the 556 nm light was distributed to deliver 20 mW for each of the two axes on the x-z plane, and 4 mW along the y axis.

III. NUMERICAL SIMULATIONS

One of the main challenges of this scheme is to operate both the singlet shell and the BB triplet core under the same magnetic field gradient condition. To first order, we could define an optimum magnetic field gradient as when the Zeeman shift becomes equal to Γ of the cooling transition at the boundary of the MOT [19]. Since $\Gamma_{399}/\Gamma_{556} \cong 154 \gg 1$, we should expect vastly different optimum magnetic field gradient values for the BB triplet-core and singlet-shell regions of the MOT. Note that this large discrepancy in natural linewidths for the singlet and triplet transitions can be generally applied to all AEML atoms. Understanding this problem, we numerically simulate the atomic capture process of our scheme to search for a set of magnetic field gradient and laser frequency detuning parameters which maximizes the overall loading rate for the core-shell MOT.

In order to simulate the loading rate of a MOT, the radiation force experienced by the atoms is calculated in terms of the saturation parameter I/I_{sat} for the singlet (s_{399}) and the triplet (s_{556}) transitions, the laser detunings for the singlet ($\delta_{L,399}$) and the triplet ($\delta_{L,556}$) transitions, and the magnetic field gradient (dB/dz). Figure 2 shows the calculated radiation force along the z direction of the BB triplet MOT by considering a two-level atom interacting with multiple light

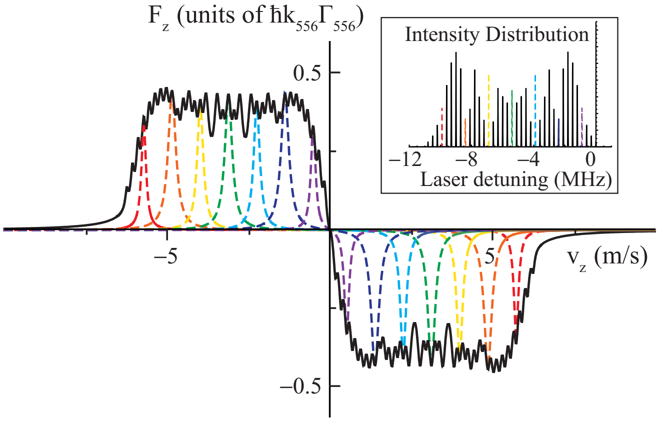

FIG. 2. (Color online) Calculated velocity-dependent radiation force for the BB triplet transition under typical experimental conditions of $s_{556} = 400$, $\delta_{L,556} = -5.4$ MHz, $dB/dz = 5$ G/cm, and the laser frequency broadened as shown in the inset. Inset: The light-intensity distribution of the BB triplet transition where the modulation frequency is $f_m = 300$ kHz and the modulation index is $H = 13$. The dashed lines in different colors show the multiple radiation force terms coming from seven sampled frequency components of the BB triplet transition. The black solid line shows the total radiation force coming from all frequency components.

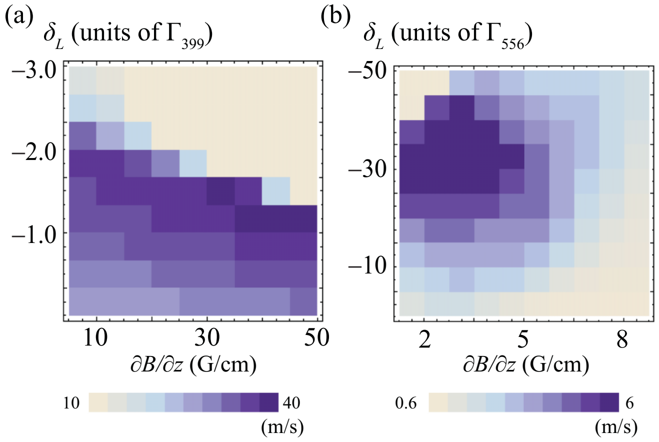

FIG. 3. (Color online) Numerically simulated capture velocities under various $\partial B/\partial z$ and δ_L for (a) the singlet transition and (b) the broadband triplet transition under the typical experimental conditions described in the text.

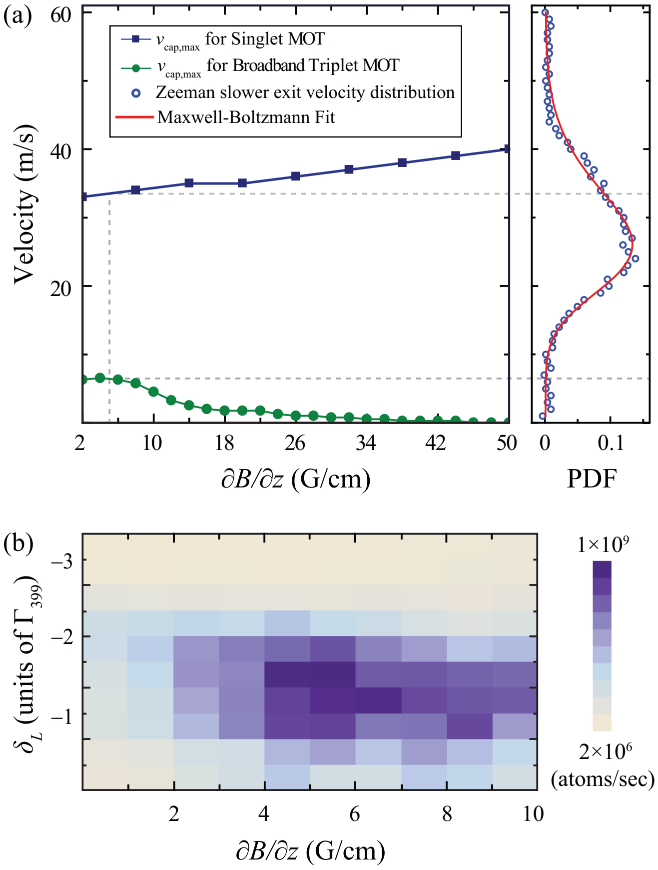

FIG. 4. (Color online) (a) Numerically simulated maximum capture velocity, $v_{\mathrm{cap,max}}$, which is the largest capture velocity obtainable at a fixed $\partial B/\partial z$ and a given laser intensity, for both the singlet and the broadband triplet transition (left). Measured axial atomic velocity distribution after the Zeeman slower (right). Dashed gray lines mark $v_{\mathrm{cap,max}}$ at $\partial B/\partial z = 5$ G/cm and the corresponding values of the velocity distribution. (b) Experimentally measured core-shell MOT loading rates under the conditions described in the text.

fields at different detunings [20]. We can compare Fig. 2 with the calculated velocity-dependent radiation force for the singlet MOT under typical experimental conditions of $s_{399} = 0.32$, $\delta_{L,399} = -45$ MHz, and $dB/dz = 5$ G/cm. The radiation force from the singlet MOT peaks for atoms with velocity $v_z = 10$ m/s where it is $\sim$60 times larger than the peak radiation force for the broadband triplet transition. This large discrepancy can be mainly attributed to the large difference of Γ between the two transitions. Due to the spatial arrangement of the light fields in our core-shell MOT scheme, the higher velocity atoms near the edge of the MOT are affected only by the strong singlet-transition radiation force. On the other hand, the cooling properties of the lower velocity atoms near the center of the MOT are completely determined by the BB triplet transition.

Given the calculated radiation force exerting on an atom with a specific position and velocity, we could numerically simulate the atomic movement inside the trapping region and find the capture velocity, v_{cap}, as a function of $\partial B/\partial z$ and δ_L. The radiation force is applied in a discrete fashion to an atom with a displacement $\vec{d}_n$ away from the MOT center and a velocity $\vec{v}_n$, where the subscript n denotes the nth iteration of the simulation. This information is then used to calculate the next iterative step of the simulation, $\vec{d}_{n+1}$ and $\vec{v}_{n+1}$. The atom is initially positioned outside of the MOT region with a velocity of v_{slower} along the z axis, which illustrates an atom exiting the Zeeman slower. We iteratively apply the radiation force in time steps set to the inverse of the spontaneous emission rate of the transition. We continue the iterations until the magnitude of the velocity $\vec{v}_n$ is less than the Doppler limited velocity of the transition (implying successful capture) or the displacement $\vec{d}_n$ steps outside the spherical boundary of the laser beam (implying failure of capture). With this numerical simulation tool, we could retrieve the largest initial velocity v_0^* of atoms that are captured. We define this as the capture velocity, v_{cap}, for the corresponding set of simulation conditions.

We plot the simulated capture velocities for the singlet MOT in Fig. 3(a) and that for the broadband triplet MOT in Fig. 3(b). There are two control parameters in each plot, which are the magnetic field gradient ($\partial B/\partial z$) and the laser frequency detuning (δ_L) for the MOT, while fixing all the other parameters as described previously. The highest capture velocity of the singlet MOT is 40 m/s with $\partial B/\partial z = 50$ G/cm, while the BB triplet MOT capture velocity peaks at 6 m/s with $\partial B/\partial z = 4$ G/cm. The difference in the maximum capture velocities and the optimum $\partial B/\partial z$ values can be qualitatively understood by its relation to the natural linewidth.

We further calculate $v_{\mathrm{cap,max}}$, which is defined as the highest capture velocity obtainable by optimization of δ_L for a given laser intensity, as a function of $\partial B/\partial z$. Figure 4(a) shows the calculated $v_{\mathrm{cap,max}}$ for the singlet and the BB triplet MOT (on the left side), along with the measured axial atomic velocity distribution after the Zeeman slower (on the right side). As expected from the difference in Γ between the two transitions, $v_{\mathrm{cap,max}}$ is maximized at very different magnetic field gradient values of 50 and 4 G/cm, for the singlet and BB triplet MOTs. For the singlet MOT, $v_{\mathrm{cap,max}}$ only changes about 20% for the range of $\partial B/\partial z$ studied here. On the other hand, $v_{\mathrm{cap,max}}$ for the BB triplet MOT decreases by more than a factor of 2 when $\partial B/\partial z > 10$ G/cm compared to when $\partial B/\partial z$ is

2–6 G/cm. The relative insensitivity of $v_{\text{cap,max}}$ with respect to the magnetic field gradient for the singlet MOT originates from Γ being large, which allows the atoms to be affected by the scattering force for a larger range of B-field conditions. These results imply that one can operate the core-shell MOT closer to the optimum magnetic field gradient of the BB triplet MOT without much loss of capturing performance from the singlet shell.

IV. RESULTS AND DISCUSSION

A. Core-shell MOT loading performance

The information obtained from Fig. 4(a) suggests an experimental search range for δ_L and $\partial B/\partial z$ values, which would give the highest loading rate and maximum trapped atom number for the core-shell MOT scheme. Figure 4(b) shows the core-shell MOT loading rates measured by observing the fluorescence from the triplet transition with a photomultiplying tube under various experimental conditions. We fixed the laser parameters of the BB triplet core at $s_{556} = 400$, $\delta_{L,556} = -5.4$ MHz, $f_m = 300$ kHz, $H = 13$, while varying $\partial B/\partial z$ and $\delta_{L,399}$ of the singlet shell. The diameter of the circular mask, which is used for blocking the center of the singlet MOT beams, was 4 mm. The measured core-shell MOT loading rate was maximized at $\partial B/\partial z = 5$ G/cm, which is within the range of the field gradient for high $v_{\text{cap,max}}$ in the BB triplet MOT.

Figure 5 shows the MOT loading process measured for the core-shell MOT and the BB triplet MOT, both at their optimized conditions. The MOT loading process is described by the rate equation [21],

$$\dot{N} = L - \alpha N - \beta \int n^2(\mathbf{r}) d^3\mathbf{r}, \qquad (1)$$

where L is the loading rate, α is the linear loss rate, β is the two-body collision coefficient, $n(\mathbf{r}) = n_0 e^{-(\mathbf{r}/a)^2}$ is the atomic density distribution in the trap with n_0 as the peak density, and a represents the width of the atomic cloud. The experimental loading rates are given by $L = \alpha N_{ss} + \beta(\sqrt{2\pi}a)^{-3} N_{ss}^2$, where N_{ss} is the steady-state number. The core-shell MOT loading scheme decreases the loading time given as $\tau = N_{ss}/L$ by a factor of 19 and increases N_{ss} by a factor of 11 compared to the BB triplet MOT, which results in more than two orders of magnitude improvement of L. Such high gain in L is possible due to the nonlinearly increasing fraction of the Zeeman slowed atoms being captured as v_{cap} of the MOT increases [see Fig. 4(a)]. At the optimal setting of the core-shell MOT, we have trapped up to $N_{ss} = 1.5(3) \times 10^9$ ^{174}Yb atoms with $\tau = 1.2(3)$ seconds.

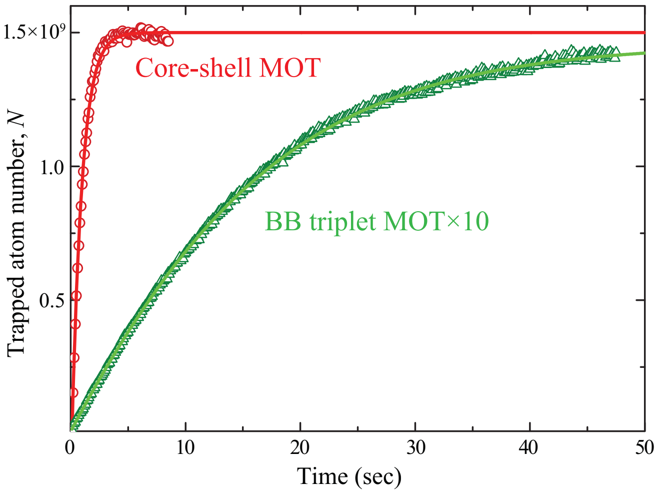

FIG. 5. (Color online) Experimental measure of the MOT loading process for the core-shell MOT and the BB triplet MOT. Solid lines are the fits. The BB triplet MOT atom number has been multiplied by 10 for viewing purposes.

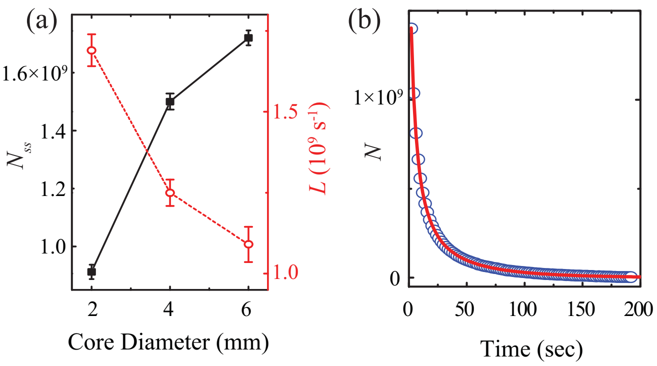

FIG. 6. (Color online) (a) Change in N_{ss} (black squares) and L (red open circles) for the core-shell MOT with different hole diameters. Error bars correspond to 2σ fitting errors. (b) Core-shell MOT atom number decay rate measurement (blue open circles) and fit (red solid line). The core diameter was 4 mm.

B. Core-shell MOT characterization

We also study how the thickness of the singlet shell versus the size of the BB triplet core of our MOT geometry affects N_{ss} and L. For this purpose, we varied the circular mask diameter which creates different size holes at the center of the singlet-transition MOT beams. The triplet-transition MOT beam diameters were changed accordingly to fill the hole, while the intensity was kept constant. Figure 6(a) shows the relative change in N_{ss} and L with three different core sizes. We observed faster loading rates as we decrease the core diameter, which is consistent with our intuition since it creates a thicker outer shell of the strong singlet transition having more cooling power. On the other hand, N_{ss} decreases with smaller central core volume. Such behavior is due to the increase in atom loss rates as the density-dependent term in Eq. (1) becomes larger.

Utilizing the fast loading of the core-shell MOT scheme, we were able to reach densities of $\gtrsim 1 \times 10^{11}$ ^{174}Yb atoms/cm^3 in the trap, which allowed us to observe the two-body collisional effects from the trap loss behavior. Figure 6(b) shows the atom number decay of the core-shell MOT, which was measured by observing the fluorescence from the triplet transition after turning off the atomic beam, the singlet-shell beams, and the modulation for the BB triplet-core beams. The singlet-shell beams were turned off to ensure that the density-dependent decay mechanism solely comes from the triplet transition. From the fit shown as a red solid line in Fig. 6(b), we get a linear loss rate of $\alpha = 0.017(1)$ s^{-1} and a two-body loss coefficient of $\beta = 4.2(5)(16) \times 10^{-12}$ cm^3 s^{-1}, where 2σ fitting errors are shown inside the first parentheses and the systematic error coming from the absolute density calibration is shown in the second parentheses. The two-body term β is closely linked to the photoassociation (PA) process. The PA process of Yb has been investigated experimentally using optical dipole traps [22,23] at different density and atom number regimes compared to this work. We believe our core-shell MOT scheme could be used to study the density-dependent trap loss rates complementing the previous results, which could provide more insight to the PA process of AEML atoms.

V. CONCLUSIONS

In this work, we have demonstrated a core-shell MOT scheme for Yb atoms where we simultaneously utilize both the singlet and the triplet cooling transitions in two spatially separated zones to achieve not only a fast-loading rate but also a high steady-state atom number in the trap. We studied how the radiation force is exerted for this type of MOT and discussed how to set the relevant parameters in order to maximize the loading efficiency. Our scheme was applied to ^{174}Yb atoms which revealed more than two orders of magnitude faster loading rate and a tenfold higher steady-state atom number compared to our BB triplet MOT. We measured the density-dependent decay behavior of the ^{174}Yb MOT and extracted the two-body loss coefficient, which is relevant to the PA process. Notably, we believe our scheme could be realized in other AEML atoms to gain similar benefits. Further investigation of the core-shell MOT scheme has the potential to reduce or even eliminate the repumping process required during the MOT stage for AEML atoms with complex energy-level structures such as radium [12] and erbium [24]. The increase in loading rate and trapped atomic number can lead to the enhancement of the statistical sensitivity in many different types of precision experiments using cold AEML atoms, such as lattice clock experiments and the electric dipole moment experiments.

ACKNOWLEDGMENTS

We thank C. Y. Park for helpful discussions. This work was supported by Korea Research Institute of Standards and Science (KRISS) creative research initiative.

---

[1] N. Hinkley, J. A. Sherman, N. B. Phillips, M. Schioppo, N. D. Lemke, K. Beloy, M. Pizzocaro, C. W. Oates, and A. D. Ludlow, Science **341**, 1215 (2013).

[2] C. Y. Park, D.-H. Yu, W.-K. Lee, S. E. Park, E. B. Kim, S. K. Lee, J. W. Cho, T. H. Yoon, J. Mun, S. J. Park, T. Y. Kwon, and S.-B. Lee, Metrologia **50**, 119 (2013).

[3] B. J. Bloom, T. L. Nicholson, J. R. Williams, S. L. Campbell, M. Bishof, X. Zhang, W. Zhang, S. L. Bromley, and J. Ye, Nature (London) **506**, 71 (2014).

[4] N. Poli, F.-Y. Wang, M. G. Tarallo, A. Alberti, M. Prevedelli, and G. M. Tino, Phys. Rev. Lett. **106**, 038501 (2011).

[5] F. Scazza, C. Hofrichter, M. Höfer, P. C. De Groot, I. Bloch, and S. Fölling, Nat. Phys. **10**, 779 (2014).

[6] X. Zhang, M. Bishof, S. L. Bromley, C. V. Kraus, M. S. Safronova, P. Zoller, A. M. Rey, and J. Ye, Science **345**, 1467 (2014).

[7] T. Rosenband, D. B. Hume, P. O. Schmidt, C. W. Chou, A. Brusch, L. Lorini, W. H. Oskay, R. E. Drullinger, T. M. Fortier, J. E. Stalnaker, S. A. Diddams, W. C. Swann, N. R. Newbury, W. M. Itano, D. J. Wineland, and J. C. Bergquist, Science **319**, 1808 (2008).

[8] C. W. Chou, D. B. Hume, T. Rosenband, and D. J. Wineland, Science **329**, 1630 (2010).

[9] A. J. Daley, M. M. Boyd, J. Ye, and P. Zoller, Phys. Rev. Lett. **101**, 170504 (2008).

[10] F. Gerbier and J. Dalibard, New J. Phys. **12**, 033007 (2010).

[11] V. Natarajan, Eur. Phys. J. D **32**, 33 (2005).

[12] J. R. Guest, N. D. Scielzo, I. Ahmad, K. Bailey, J. P. Greene, R. J. Holt, Z.-T. Lu, T. P. O'Connor, and D. H. Potterveld, Phys. Rev. Lett. **98**, 093001 (2007).

[13] T. Kuwamoto, K. Honda, Y. Takahashi, and T. Yabuzaki, Phys. Rev. A **60**, R745(R) (1999).

[14] H. Katori, T. Ido, Y. Isoya, and M. Kuwata-Gonokami, Phys. Rev. Lett. **82**, 1116 (1999).

[15] R. Maruyama, Ph.D. thesis, University of Washington, 2003.

[16] J. W. Cho, H.-G. Lee, S. Lee, J. Ahn, W.-K. Lee, D.-H. Yu, S. K. Lee, and C. Y. Park, Phys. Rev. A **85**, 035401 (2012).

[17] B. Hemmerling, G. K. Drayna, E. Chae, A. Ravi, and J. M. Doyle, New J. Phys. **16**, 063070 (2014).

[18] S. Dorscher, A. Thobe, B. Hundt, A. Kochanke, R. L. Targat, P. Windpassinger, C. Becker, and K. Sengstock, Rev. Sci. Instrum. **84**, 043109 (2013).

[19] A. M. Steane, M. Chowdhury, and C. J. Foot, J. Opt. Soc. Am. B **9**, 2142 (1992).

[20] T. Savels, A. P. Mosk, and A. Lagendijk, arXiv:cond-mat/0410661v2.

[21] T. P. Dinneen, K. R. Vogel, E. Arimondo, J. L. Hall, and A. Gallagher, Phys. Rev. A **59**, 1216 (1999).

[22] Y. Takasu, K. Komori, K. Honda, M. Kumakura, T. Yabuzaki, and Y. Takahashi, Phys. Rev. Lett. **93**, 123202 (2004).

[23] K. Enomoto, K. Kasa, M. Kitagawa, and Y. Takahashi, Phys. Rev. Lett. **101**, 203201 (2008).

[24] A. Frisch, K. Aikawa, M. Mark, A. Rietzler, J. Schindler, E. Zupanic, R. Grimm, and F. Ferlaino, Phys. Rev. A **85**, 051401 (2012).